Supplementary data for Article

This file contains experimental protocols and characterization data used by the various laboratories

Table of contents

1 Nomenclature of degradation stages of cement systems used in the present work

This paper closely follows the denotation of cement degradation upon water access to the solid as proposed by (Ochs et al., 2016), illustrating the indicative evolution of pH at 25 °C in hydrated cement pore fluid as a result of cement degradation. The notion of "cement degradation" refers here to the change of the phase assemblage constituting the cement caused by the frequent exchange of cement pore water with the ground water of the surrounding disposal environment, expressed as "pore water exchange cycles". The solution composition in stage I is the non-degraded state and is controlled by soluble sodium (Na) and potassium (K) salts leading to pore water pH values between 12.5 and 13.5. The first degradation state is stage II characterized by equilibrium of the pore water solution with portlandite ($Ca(OH)_2$) leading to a fixed pH of about 12.5. Further exchange cycles of pore water lead to stage III of degradation characterized by the disappearance (by dissolution) of portlandite and control of pore water solution composition (in particular of Ca and Si concentrations) by equilibria with calcium silica hydrate (CSH) phases. As CSH phases have to a certain degree a variable composition (a variable Ca/Si ratio), stage III covers the evolution of pore water pH values from 12.5 to about 10 with increasing pore water exchange cycles accompanied by a change of the Ca/Si ratio of the CSH phases from 1.7 to 0.8. In the present work we defined a further subdivision of stage III into a stage III.a with a pH of about 12 and a stage III.b with a pH of 11.3. Finally, at an even larger extent of pore water exchange a stage IV is reached with a pH below 10, characterized by the disappearance of CSH phases and solution control by residual minerals (in the present case, calcite).

2 Laboratory RATEN

2.1 Materials and mehods

Hardened cement pastes (HCP) based on CEM I 52.5 (OPC, LAFARGE, Val d'Azergues factory) and CEM V/A 32.5 (blast furnace slag and fly ash added to OPC, HOLCIM, Heming factory) cement were studied in RATEN ICN in the frame of CEBAMA project. These HCPs were prepared with a water/cement ratio of 0.38 and were received in 2016 from ARMINES as alteration stage II, where these pastes were kept for almost 7 years after setting in saturated portlandite water (pH = 12.4), at 20°C to avoid their carbonation, since the CO_2 dissolved in saturated portlandite water (prepared with degassed deionized water) is significant lower that CO_2 in atmospheric conditions and cement carbonation is slower in aqueous solution. Between receiving time and using them in degradation and sorption tests, the HCPs were also kept in saturated portlandite water at room temperature (20±3°C).

The slices of the two HCPs were crushed and sieved under nitrogen atmosphere (using nitrogen of 99.99 purity) and the 125 – 250 μm fractions were kept both for sorption tests and to prepare three degraded states of the cement pastes. The first two degradation states (Stage III.a at pH 12.03 and Stage III.b at pH 11.3) were obtained by hydrolysis leaching process (15 days) in degassed deionized water (DDW) at two solid to water ratios: ~ 3.7 g/l for the first degradation state and 0.4 g/l for the second one ((Pointeau et al., 2004). A more aggressive degradation protocol was applied to obtain the third degradation state (Stage IV apH 9.28). The cement pastes were first mixed with ammonium nitrate solution (S/V ratio of 7.8 g/l) to accelerate the chemical degradation and after that the calcium was leached in DDW, at S/V ratio of 0.01 g/l (after contacting with NH_4NO_3 the cement pastes were washed four times with DDW, until the pH of solution was constant).

A stock solution with C-14 in carbonate form ($Na_2{}^{14}CO_3$ in NaOH 2M, with specific activity of 1 mCi/g, IFIN-HH Bucharest) and a Ra-226 standard solution (water solution of barium and radium chlorides in HCl, with Ra-226 specific activity of 0.9016 mCi/g, EUROSTANDARD CZ) were used to prepare de contact solutions for batch sorption tests.

Since the two cement pastes were kept in saturated portlandite water for ~ 9 years, it was considered that this artificial cement pore water (ACW) is most suitable to prepare the contact solutions (spiked with C-14 and Ra-226, respectively) for batch sorption on non-degraded HCP, while for degraded pastes, the waters resulted from the degradation tests were used to prepare spiked solutions for sorption tests.

The influence of cement degradation on C-14 and Ra-226 uptake were studied by batch sorption/desorption tests carried on non-degraded cement pastes (based on CEM I and CEM V) and three degraded cement pastes (Stage III.a, Stage III.b and Stage IV). The batch tests were carried out at a solid to liquid ratio of 2.5 g/L(expressed as dry mass determined by ignition of HCP at 1100°C), at room temperature (23±3°C) in polypropylene centrifuge tubes. Before use, the PP tubes were prewashed in 0.1M HNO_3 and thoroughly rinsed with deionized water. All experiments were carried out in duplicate samples and cement paste weighting, batch preparation, and supernatant sampling were performed under nitrogen atmosphere. Blank batches were prepared for measuring the C-14 and respectively Ra-226 content the cement pastes and also the radionuclide sorption on the tubes walls was checked. Desorption tests complemented the sorption ones in order to evaluate the reversibility of C-14 and Ra-226 on HCPs.

Before adding the C-14 and respectively Ra-226, respectively spiked solutions, all HCP samples were pre-equilibrated with 8 ml of corresponding ACW for 24 hours, and after this pre-equilibration time, the spiked solutions were added.

. During the pre-equilibration and equilibration time, the test tubes were gently shaken (horizontally placed on an orbital shaker), at 100 rpm. After equilibration the test tubes were centrifuged at 19620 g (11000 rpm) for 40 min. The supernatant was separated and the residual activity of C-14 and respectively Ra-226 in the batch solutions was measured. The C-14 measurements were performed by liquid scintillation counting, with Hionic Fluor liquid scintillation cocktail (for sample to scintillation cocktail ratio of 1 to 10), using counter model 4910 TRICARB Perkin Elmer. Ra-226 measurements were achieved by alpha-LSC method, based on the absorption of the Rn-222 resulted by Ra-226 decay into an immiscible organic scintillator (UltimaGold F) and counting of the alpha-particles emission of Rn-222 and its short-lived daughters (Po-218 and Po-214) using a liquid scintillation counter with alpha-beta discrimination. For each batch solution, two parallel LSC counting vials were measured with a sample to scintillation cocktail ratio of 1 to 10 and 1 to 1, for C-14 and Ra-226, respectively.

2.2 Characterizations

To correlate the sorption data with the main phases present in the cement pastes, XRD investigations were carried out. These measurements show that as it was expected, the degraded pastes are indeed free of portlandite (Figure 2.2-1). This was also sustained by the TGA analyses that show that the mass loss between 400-600°C, the characteristic range for portlandite decomposition) is lower in all three degraded phases compared to the no-degraded one.

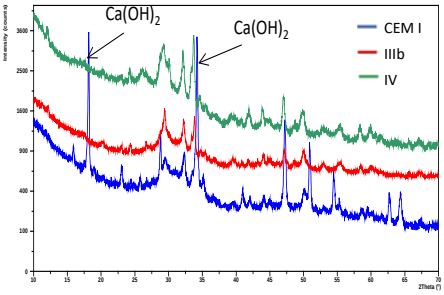

main phase identified, wt%	non-degraded	III.a	III.b	IV
Portlandite Ca(O H)2	24	1	1	1
Ettringite Ca6 (Al (O H)6)2 (S O4)3 (H2 O)26	16	18	19	23
Tobermorite Ca3 (Si2O6 (OH)2) (H2O)	8			
Tobermorite13A Ca12 (Si8O28) (H2O)13	8	15	14	24
Tobermorite11A Ca2.25 Si3 O7.5 (O H)1.5 (H2 O)	7			
Tobermorite 9A Ca5 Si6 O16 (O H)2	28	16	19	12
Tobermorite 12.5 A Ca7.76 Si6.76 O18.8 (O H)4.88 (H2 O)7.84		9	7	
Clinotobermorite Ca5 Si6 O17 (H2 O)5		16	15	13
Aklimaite Ca4 (Si2O5 (OH)2)(OH)4(H2O)5	8			
Okenite Ca5 Si9 O23 (H2 O)9		24	26	

temperature interval, °C	mass loss, % CEM I			
	non-degraded	IIIa	IIIb	IV
22-200 (water)	13.92	10.06	13.13	10.87
200-400 (Ca hydroxy-aluminates)	4.152	5.43	6.99	3.52
400 - 600 Calcium hydroxide	5.83	3.307	2.54	0.739
600-800 (partial carbonation of Ca hydroxy-aluminates)	0.984	1.709	2.815	0.726
800-1000 (cristalyne Ca from admixtures)	0.323	0.054	0.289	0.172
total mass loss	**25.214**	**19.793**	**26.531**	**16.027**

Figure 2.2-1. *XRD spectra and the main phases identified in non-degraded and degraded CEM I pastes phases (Stage III.a and III.b and Stage IV) and the mass loss measured by TGA*

The extent of Ca content (as it has a strong influence on the uptake of anionic species) in the non-degraded and degraded cement pastes was determined by emission spectrometry carried out on samples resulted by cement pastes dissolution (microwave digestion in HNO_3, HCl and HF). As it was expected, the HCP based on CEM V contain less Ca than the one base on CEM I, mainly due to the lower clinker content of CEM V that has blast furnace slag and fly ash added to the OPC (Table 2.2.1). Also, the Ca content in degraded pastes is lower compared with non-degraded ones. These data were also confirmed by EDS investigations, both on non-degraded and degraded cement pastes.

Table 2.2.1. *Oxide composition of the cement pastes used in sorption/desorption tests*

Main oxide content, %	**CEM I**				**CEM V**			
	CEM I non-degraded	CEM I_ Stage III.a	CEM I_ Stage III.b	CEM I_ Stage IV	CEM V non-degraded	CEM V_ Stage III.a	CEM V_ Stage III.b	CEM V_ Stage IV
CaO	49.57	37.26	35.04	22.91	36.52	29.49	26.78	25.31
SiO_2	16.53	16.58	16.54	16.55	22.90	22.90	22.90	22.90
Al_2O_3	4.13	4.28	4.17	4.55	8.53	8.49	8.63	7.71
C/S ratio	**2.99**	**2.25**	**2.12**	**1.38**	**1.59**	**1.29**	**1.17**	**1.11**

3 Laboratory CTU

3.1 Materials and methods

The methodology of sorption on crushed hydrated cement paste (prepared with water/cement ratio w = 0.667) in our laboratory was implemented via the study of the ^{85}Sr uptake during preliminary sorption experiments on a cement of CEM II grade. CEM II/A-S 42.5 R (produced by Lafarge Cement, a. s.) was chosen for the study of sorption behavior of strontium that served as an analog of radium. As a liquid phase, leachate of the hydrated cement paste (V/m = 5 L/kg, contact time 1 month, pH = 12.8) was then used. Afterwards, first sorption experiments with ^{223}Ra (gained via $^{227}Ac/^{227}Th/^{223}Ra$ generator) were performed also on another cement of type CEM II (CEM II/B-M (S-LL) 32.5 R - produced by Českomoravský cement, a. s.; Heidelberg Cement Group). This material is Portland composite cement of the strength class made of clinker, granulated blast furnace slag (approx. 15 %), of limestone (approx. 12 %), and with low TOC content and anhydrite as retarder, and was utilized only in the orientation stage of the work. On the other hand, the cement CEM II/A-S 42.5 R (hydration for 6 months) was used throughout the project. This cement material is made by grinding together silicate clinker, blast furnace granulated slag (max. 20 %) and gypsum. Also retardation properties of other cementitious materials were studied – a concrete containing the type of cement CEM I 42.5 (with fine and rough aggregate and fly ash, hydration for 1 month) utilized in ÚJV Řež a.s. to stabilize the solidified solid waste container, and a concrete with the type of cement CEM III B/32.5 (produced by CEMEX Czech Republic, s.r.o., with fine and rough aggregate, hydration for 1 month) used to fill chambers in intermediate radioactive waste repository Richard. All solid materials were prepared in the form of blocks hydrated in a highly humid environment for at least 19 days. For sorption and diffusion experiments these prepared hydrated materials were crushed and sieved for fraction ≤ 0.4 mm and contacted with two types of liquid phases with initial pH around 12.5: filtered saturated $Ca(OH)_2$ (Portlandite water) and the synthetic cement pore water (CPW) with a composition that represents a deeper circulation of groundwater (Table 3.1) in the fissure environment of the crystalline rocks of the Bohemian Massif mixed with saturated $Ca(OH)_2$.

Table 3.1: *Composition of synthetic granite groundwater*

Ion	Na^+	K^+	Mg^{2+}	Ca^{2+}	Cl^-	F^-	HCO_3^-	SO_4^{2-}	NO_3^-	PO_4^{3-}
c [mmol/L]	0.71	0.05	0.35	0.88	0.09	0.02	2.7	0.19	0.03	0.04

3.2 Characterizations

Cementitious materials CEM II/A-S 42.5 R and CEM II/B-M (S-LL) 32.5 R were characterized by pycnometric method, B.E.T., FTIR, and X-ray diffraction. Both materials differ significantly, particularly in the specific surface area and composition. Density of hydrated cement paste made of CEM II/A-S 42.5 R was determined as equal to 2177 ± 44 kg/m^3 by a pycnometric method on crushed material. Specific surface area obtained value by the means of the rapid dynamic flow method for determinations of single-point B.E.T. was 20.1 ± 0.3 m^2/g. The comparison of measured spectrum by X-ray diffraction with database ICDD PDF-2 (version 2013) enabled to identify four mineral phases, namely calcite $CaCO_3$, portlandite $Ca(OH)_2$, hydrotalcite $Mg_6Al_2CO_3(OH)_{16}{\cdot}4(H_2O)$ and ettringite $Ca_6Al_2(SO_4)_3(OH)_{12}{\cdot}26H_2O$. FTIR spectra were obtained using the Attenuated Total Reflection (ATR) technique in the scan range of 400 – 4000 cm^{-1}. Leaching of hydrated cement paste to water (V/m = 10 L/kg) for 3 months caused only a very small change in the FTIR spectrum. For the CEM II/B-M (S-LL) 32.5 R hydrated cement paste the results were: density - 1998 ± 29 kg/m^3, specific surface area 48.5 ± 0.3 m^2/g, only calcite and portlandite identified by X-ray diffraction. Findings valid for FTIR are the same for both cement materials. Also characteristics of both concrete materials (Concrete UJV and Concrete Richard) were determined. By means of X-ray diffraction, portlandite $Ca(OH)_2$ and quartz SiO_2 presence was confirmed. Value of specific surface area was
12,65 ± 1.3 m^2/g for Concrete UJV; and 8.37 ± 0.2 m^2/g for Concrete Richard. The mass of solid phase used in the experiments was corrected for the moisture content (determined after 3 days drying at 105 °C).

4 Laboratory Amphos21

4.1 Materials and methods

C-S-H phases with three different Ca/Si ratios were individually synthesized using a solid to liquid (S/L) ratio of 20 g/L with SiO_2 and CaO as starting materials. Once weighted, the solids were mixed with DDW (deionized degassed water) and equilibrated during at least 20 days. The whole synthesis procedure was carried out inside a glovebox filled with N_2 99.99999%.

AFt phase (Ettringite: $Ca_6(Al,Fe)_2X_3(OH)_{12}{\cdot}xH_2O$, X being one divalent or two monovalent anions) was synthesized from CaO and $Al_2(SO_4)_3{\cdot}18\ H_2O$ by a hydrothermal procedure at 60°C under N_2 (g) atmosphere to avoid carbonation following the procedure described in (Perkins and Palmer, 1999). AFt corresponding solid and aqueous phases were fully characterized and identified as AFt pure phase.

AFm/AFt mixtures with variable SO_3/Al_2O_3 ratios (namely S0.5, S1, S2 and S2.5) were synthesized by mixing the appropriate amounts of C_3A, CaO, $CaSO_4$ and $CaCO_3$ and equilibrating the mixtures in DDW for 25 days.

4.2 Characterizations

Obtained **CSH phases**, together with their equilibrated waters were extensively analysed by different techniques to clearly characterize their structural and compositional features. The results obtained from characterization agreed with the expected composition as well as with most of the results reported in bibliography for solids with similar composition. Water content increased with the Ca/Si ratio, surface specific area followed the opposite trend, being higher for lower Ca/Si ratios. The three solids presented similar XRD patterns characterized by the amorphous structure.

Molybdenum adsorption kinetics were evaluated as a first approach to the molybdenum adsorption studies. This kind of experiments allowed not only to stablish the time necessary to attain the equilibrium but also to identify those phases able to retain molybdenum more efficiently. The selection of the three Ca/Si ratio tested

in this work was based on literature results. Most studies indicate that surface characteristics as zeta potential of C-S-H gels vary as a function of Ca concentration or pH. In this sense, our selection includes three Ca/Si ratios, covering from negative (C-S-H 0.8) to slightly positive values (C-S-H 1.4) with C-S-H 1.2 in between, which presents near neutral charge.

From first kinetic studies, C-S-H gels with low Ca/Si ratios were discarded due to their low molybdenum retention capacity. Lower contact times were tested for C-S-H 1.4 selecting 1 day as optimum for the development of isotherm experiments.

AFt phases: The elemental analysis carried out by EDX confirmed the atomic percentages that match with AFt composition. SEM images showed the presence of only one crystal type on the sample, with typical AFt needle shape. TGA analysis allowed detecting two different types of hydration water, the first one corresponding to water molecules located on the outer surface of AFt, the second one was attributed to the dehydration of aluminums hydroxide. The aqueous fraction was mainly composed by sulphate anions (~7 mM) and calcium (~4 mM). Molybdenum retention onto AFt phase was evaluated by analysing the results derived from kinetic studies.

AFm/Aft mixtures: The results obtained from the characterization using different analytical techniques were consistent with each other, which suggest the reliability and consistency of the experimental method. AFm and AFt phases precipitated as totally different phases, therefore no solid solution was observed to form between these two phases in the present study. A marked division of the synthesised samples can be observed with a significant different structural composition, i.e. major AFt content in the samples of S(VI)/Al equal to 2 and 2.5, and major AFm content in the samples of ratio 1 and 0.5, as can be drawn from SEM micrographs shown in ***Figure*** 4.1.

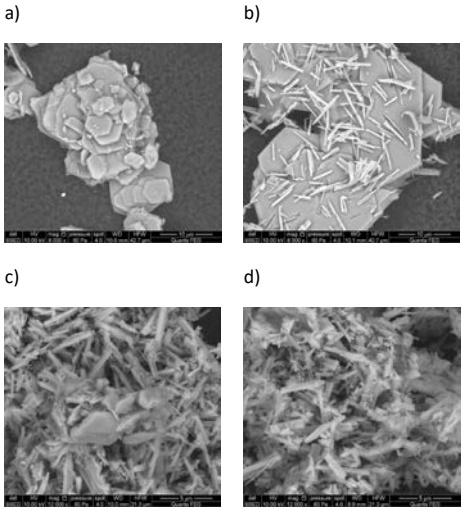

Figure 4.1. *Micrographs of synthesised mixed samples at 6kx. S(VI)/Al ratios a) 0.5, b) 1, c) 2, d) 2.5.*

From XRD patterns summarized in Figure 4.2 the monosulphate precipitation seems to take place in all the synthesised samples regardless the amount of sulphate in the system. In turn, no ettringite was observed in samples of initial ratio S(VI)/Al = 0.5 (Sample S0.5), whereas in the rest of samples, ettringite and monosulphate coexist. Some impurities are also detected in the synthesised samples, such as gypsum in S2 and S2.5 due to

the high sulphate content, or hydrogarnet in S0.5. Likewise, although the presence of carbonate has been avoided, some limited monocarbonate and/or hemicarbonate precipitation also occurs in the samples.

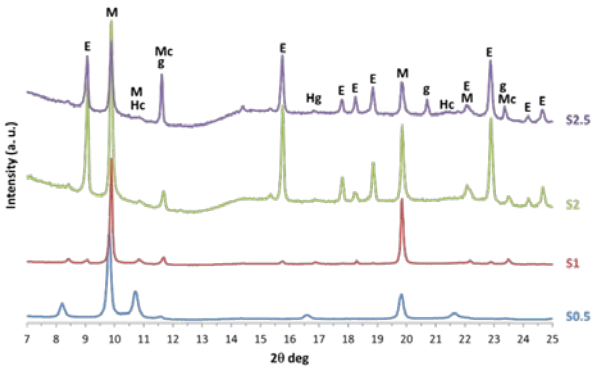

Figure 4.2 *X-Ray powder diffraction spectra of synthesised mixed phases. M – monosulphoaluminate; E – ettringite; Mc – monocarbonate; Hc – hemicarbonate; g – gypsum; Hg – Hydrogarnet (C_3AH_6).*

5 Laboratory KIT

5.1 Materials and methods

Solubility studies

Solubility experiments were performed under Ar-atmosphere at T = (22 ± 2) °C. Two different solid phases were investigated: BeO(cr) (commercial) and α-$Be(OH)_2$(cr) (synthesized in this work). The hydroxide phase was prepared by slow titration under continuous agitation of a 0.35 M BeSO4 solution with 2.0 M carbonate-free NaOH solution up to pH ≈ 10.5. The original amorphous phase was equilibrated for up to 600 days until complete conversion to α-$Be(OH)_2$(cr). The following solubility systems were investigated:

Absence of carbonate

- 0.1–5.0 M NaCl–NaOH, 5 series, with $5 \leq pH_m \leq 14.5$
- 0.1–4.0 M KCl–KOH, 5 series, with $9 \leq pH_m \leq 14.3$
- 0.01–4.0 M NaOH
- 0.01–4.0 M KOH

Presence of carbonate

- 0.5 M NaCl with C_{tot} = 0.01 and 0.1 M
- 5.0 M NaCl with C_{tot} = 0.1 and 0.4 M

Sorption studies

- Ordinary Portland cement paste (CEM I 42,5 N BV/SR/LA type), degradation stage I (pH ≈ 13). Batch sorption experiment conducted with 10^{-6} M ≤ $[Be(II)]_0$ ≤ $10^{-2.5}$ M and 2 g·L^{-1} ≤ [S/L] ≤ 50 g·L^{-1}.
- Ordinary Portland cement paste (CEM I 42,5 N BV/SR/LA type), degradation stage II (pH ≈ 12.5).. Batch sorption experiment conducted with 10^{-6} M ≤ $[Be(II)]_0$ ≤ 10^{-2} M and [S/L]= 2 g·L^{-1}.
- Cebama low-pH cement paste (VTT). Batch sorption experiment conducted with 10^{-6} M ≤ $[Be(II)]_0$ ≤ 10^{-3} M and 0.2 g·L^{-1} ≤ [S/L] ≤ 2 g·L^{-1}.
- C-S-H Ca/Si = 0.6 (provided by BRGM). Batch sorption experiment conducted with 10^{-6} M ≤ $[Be(II)]_0$ ≤ 10^{-3} M and 0.2 g·L^{-1} ≤ [S/L] ≤ 2 g·L^{-1}.
- C-S-H Ca/Si = 1.0 (provided by BRGM). Batch sorption experiment conducted with 10^{-6} M ≤ $[Be(II)]_0$ ≤ $10^{-2.5}$ M and [S/L]= 2 g·L^{-1}.
- C-S-H Ca/Si = 1.6 (provided by BRGM). Batch sorption experiment conducted with 10^{-6} M ≤ $[Be(II)]_0$ ≤ $10^{-2.5}$ M and [S/L]= 2 g·L^{-1}.

5.2 Solid phase characterization

Figure 5.1 shows the XRD patterns of BeO(cr) and α-$Be(OH)_2$(cr) solid phases used in this study. The patterns collected for these solid phases perfectly match those available in the literature.

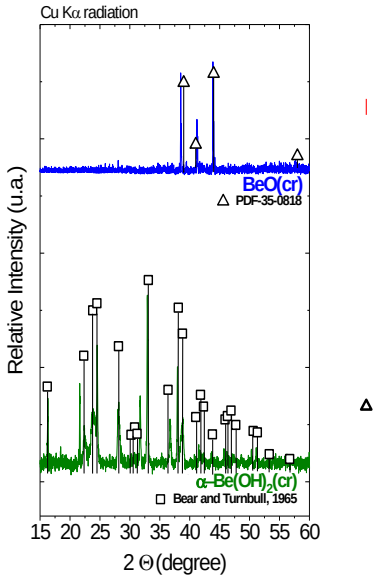

Figure 5.1. *XRD patterns of BeO(cr) and α-$Be(OH)_2$(cr) solid phases used in this study. Reference patterns shown in the figure as reported in the* (JCPDS, 2001) *database and* (Bear and Turnbull, 1965).

6 Laboratory SUBATECH/ARMINES

6.1 Materials and methods

HCP samples used were disks (2 mm thick) of a CEM V/A hardened cement paste (HCP) prepared with a water to cement ratio of 0.43 and cured at least 27 months in an artificial cement pore water (ACW ; pH~13.5) (Savoye et al., 2018). The drying stage consisted of storing HCP samples during several months (20±1°C under Ar atmosphere) at fixed relative humidity (RH) imposed by saturated saline solutions (80%, 70% and 55% RH). Thus, the initial S_w values were 0.85, 0.72 and 0.63 respectively. Afterward, HCP samples were resaturated with ACW (under vaccum). Additionally, a fully saturated sample was used as a reference. Carbonated samples were prepared in conditions representative of atmospheric carbonation (Auroy et al., 2015). An accelerated carbonation process was performed in a climatic chamber (P_{CO2} = 3% vol ; RH=55 % in order to obtain a maximal carbonation rate). Mineralogical changes induced by carbonation were highlighted by XRD analysis. Carbonation process leads to the dissolution of hydrates phases (mainly Portlandite and C-S-H) and the precipitation of calcite (from Portlandite) and but also vaterite (from C-S-H phases). These results are consistent with recent literature data (Auroy et al., 2018). Through-diffusion experiments (TD) were performed, in duplicate, using standard two-reservoir set-ups. The effective diffusion coefficient, D_e(HTO) and material capacity factor, □ were obtained by modelling the HTO cumulative activity curves (in the downstream reservoir) with a routine based on an analytical solution of Fick laws (with fixed initial and boundary conditions). For TD experiments in unsaturated condition, the osmotic technique was used for imposing a high S_w (0,84). This technique consists of generating a water suction by an osmosis process between cement pore water and a highly concentrated solution of polyethylene glycol PEG (Savoye et al., 2010). HCP samples are separated from a PEG solution by a semi-permeable membrane (permeable to water molecules and all dissolved species but PEG). The exclusion of PEG from the sample pore water produces a chemical potential imbalance between the pore water and the external solution. This osmotic suction has the effect of keeping the sample partially saturated. A mass concentration of 0.95 kg of PEG/$kg_{solution}$ has been chosen in order to reach a maximal suction potential of 9 MPa leading to a Sw value of 0.84. HCP samples used for these experiments were conditionned beforehand at 55% RH. C-14 batch experiments were carried out at ambient temperature (20 ± 1°C) in polypropylene tubes with a solid to liquid ratio of 25 g/L. Samples were pre-equilibrated in ACW pore water for one week before C-14 ($NaH^{14}CO_3$) spike addition. Before sampling, tubes were centrifuged (2650g, 30 min) and supernatants aliquots were sampled, weighted and analyzed by beta liquid scintillation counting. Quantitative C-14 measurement were performed by using a LS cocktail specifically dedicated to measurements in alkaline solution (Hionic Fluor®,Packard). For desorption experiments, at the end of the sorption step, supernatants were replaced by the same volume of ACW (free of C-14). Preparation (except for carbonated HCP) and experiments were performed in a glove box (under Ar) in order to avoid atmospheric carbonation.

Through diffusion experiments were performed for determining HTO diffusion parameters for three different conditions. The effects of a drying/rewetting cycle and of an unsaturated condition (Sw = 085) were investigated on fresh non-carbonated HCP whereas the effect of carbonation was investigated on fresh carbonated HCP. Transport parameters (effective diffusion coefficient, D_e(HTO) and material capacity factor (α)) are determined by modelling the normalized cumulative activity in the downstream reservoir with a least-square fitting based on Crank analytical solution (Crank, 1975) (Eq.1).

$$Q(t) = \frac{q(t)}{L * S * A_0} = D_e \frac{t}{L^2} - \frac{\alpha}{6} - \frac{2\alpha}{\pi^2} \sum_{n=1}^{\infty} \frac{(-1)^n}{n^2} e^{\left(-\frac{D_e n^2 \pi^2 t}{\alpha L^2}\right)} \qquad \textit{Eq. 5.1}$$

where Q(t) is the normalized total cumulative activity (Bq), q(t) is the normalized cumulative activity in the downstream reservoir (Bq), A_0 the initial activity per volume unit in the upstream reservoir ($Bq.m^{-3}$); t, the time (s); D_e, the effective diffusion coefficient ($m^2.s^{-1}$) and □ the material capacity factor (-).

In our experimental conditions, the steady-stare diffusive flux is achieved after 100 days for most of experiments. As an example, the normalized cumulative activity curve of the reference sample (fully hydrated non-carbonated HCP) is given Figure 6.1.

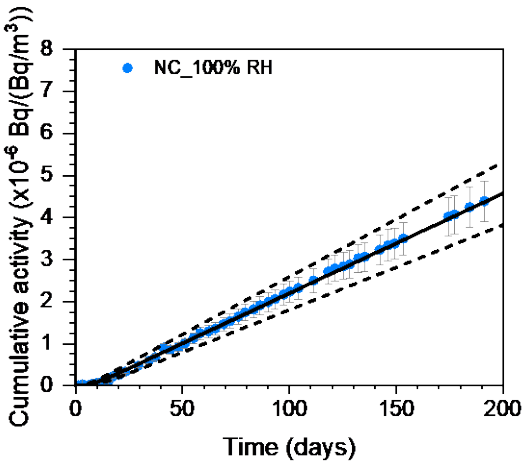

Figure 6.1. Normalized cumulative curve for HTO (reference sample). Experimental points (in blue), modelling (black solid line), uncertainties ranges (black dotted line)

7 Laboratory BRGM

7.1 Solid analyses

High-energy X-ray diffraction data were collected at station CRISTAL from SOLEIL synchrotron (Saint-Aubin, France). An electron probe microanalyzer (EPMA) was used to determine the chemical composition before and after experiments. Powder X-ray diffraction was performed with a Bruker D8 Advance diffractometer, equipped with a Cu anode (λ = 1.5418 Å) and a LynxEye detector. To protect samples from alteration by atmospheric CO_2 during measurement, powders were measured in polyimide capillaries (diameter of 1.6 mm) sealed on both sides by glue. AFm was analyzed using transmission electron microscopy (TEM) and energy dispersive X-ray spectrometry (EDX). High resolution transmission electron microscopy images were taken using a CM20 PHILIPS operating at 200 kV and having a line resolution of 1.4 Å. The gas-adsorption experiments using nitrogen as the adsorbent were conducted at 77K on a Quantachrome Nova 2200e surface area analyzer.

7.2 Solution analyses

The pH was monitored using a Metrohm electrode connected to a Mettler Toledo pH meter, which was calibrated before each experiment. Cl analyses were carried out using ion chromatography (Thermo-Dionex ICS3000). Ca, Na, and K concentrations were measured using an ICP-AES (OPTIMA 5300 DV, Perkin Elmer). Al, Se and Mo concentrations were measured using an ICP-MS (NEXION 350 X, Perkin Elmer).

7.3 Flow through method

Dissolution experiments been carried out on AFm-Cl using flow-through reactors at room temperature (Fig. 7.1). The total volume of reactors available in the BRGM laboratory is about 83 mL. An input buffer solution will circulate at a constant flow rate of about 0.5 mL min^{-1} through the reactors using a peristaltic pump (Watson Marlow, 205U). The input solution will be continuously cooled under a N_2 flux. The objective here was to suppress the CO_2 partial pressure in order to avoid carbonation during dissolution experiments (e.g. Goñi and Guerrero, 2003). The magnetic stirrer rotates on an axle in order to avoid any grinding of AFm particles between the bar and the bottom of the reactor (Metz and Ganor, 2001).

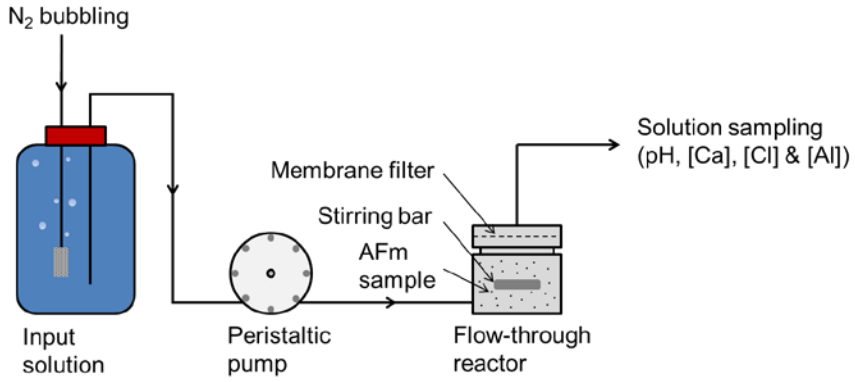

Fig. 7.1. The experimental apparatus. Figure modified from Marty et al., 2015.

7.4 Codes used for data modelling

PHREEQC3 and the THERMOCHIMIE database version 9 (Giffaut et al., 2014) were used to determine the solution saturation indices and to model the experiments.

8 Laboratory JÜLICH

The radionuclide uptake was generally determined in batch experiments performed at solid to liquid ratios S/L between 0.005 and 0.1 kg L^{-1} under anoxic conditions in a CO_2-free atmosphere in a glove box. The systems addressed comprised composite hardened cement pastes prepared from commercially available OPC (CEM I, Heidelberger Zement) as well as the CEBAMA reference low pH cement paste provided by VTT (incl. artificially carbonated cement pastes). The various model phases used in the uptake experiments were synthesized using well established procedures (i.e., C-S-H: (Atkins and Glasser, 1992); AFm: (Baur et al., 2004, Matschei et al., 2007); AFt: (Atkins et al., 1991, Baur et al., 2004); and comprised C-S-H0.9, C-S-H1.4, AFt (ettringite), AFm-SO_4, AFm-CO_3, hydrogarnet (C3AH6), calcite and portlandite; the procedures are described in detail in (Lange et al., 2018) and Lange (2019). To address various stages of cement degradation, sorption/uptake experiments with the single hydration phases were performed using different solution compositions such as equilibrium solutions, artificial young cementitious water (pH ~13.5) as well as a portlandite-saturated solution (pH ~12.5). The radionuclides/-elements used in these studies included ^{226}Ra,

$^{99}TcO_4^-$, I^-/IO_3^-, MoO_4^{-2}, and SeO_3^{-2}/SeO_4^{-2}. The tracer concentrations in solution at the end of the sorption experiments were determined either by γ-spectroscopy (^{226}Ra) using a high-purity germanium coaxial N type detector system (EGC 35-195-R, Eurisys Mesures), liquid scintillation counting (^{99}Tc) with a 1220 Ultra low level Quantulus™ LSC device (Perkin Elmer), or by ICP-MS (Elan 6100 DRC, Perkin Elmer) and ICP-OES (Thermo Scientific iCAP7600) for stable elements.

Purity and structure of the synthesised hydration phases as well as the phase assemblage of the HCP were ascertained by X-ray diffraction analyses (XRD), employing a D4 Endeavor (Bruker AXS GmbH) with a θ-2θ geometry or alternatively a D8 Advance (Bruker AXS GmbH) with a θ-θ geometry, both equipped with Cu X-ray tubes. The surface areas of the hydration phases and crushed HCP used in sorption experiments were determined by multipoint N_2-BET measurements with a Quantachrome Autosorb 1; data treatment was performed using the Quantachrome AS1Win software (v. 2.11). Microstructural investigations were carried out by SEM (FEI Quanta 200F) equipped with a field emission cathode; for energy dispersive X-ray spectroscopy (EDS), an Apollo X Silicon Drift Detector (SDD) from EDAX was used. All SEM/EDS investigations were performed in low vacuum mode (60 Pa) to avoid coating of the materials with gold or carbon. A detailed characterisation of the hydration phases and the HCP can be found in Lange et al. (2018) and Lange (2019), respectively.

To support planning and interpretation of the sorption experiments, the aqueous speciation of the components in solution and saturation indices of relevant phases were calculated with the geochemical code PhreeqC Ver. 3.4.0 (Parkhurst and Appelo, 2013) using the ANDRA ThermoChimie v.9b thermodynamic database (Giffaut et al., 2014, Grivé et al., 2015). The activities of aqueous species were calculated using the specific ion interaction (SIT) approach.

Field Code Changed

9 Laboratory University Surrey

Batch experiments were carried out on I, Se and Cl, with radium added at the request of FZ Jülich. The solids used fall into two categories: hardened cement paste (HCP) and single mineral phases. The five cement blends are: CEM I, a ground granulated blast furnace slag: ordinary Portland cement blend (GGBS:OPC), a pulverised fuel ash blend (PFA:OPC), a bespoke backfill material (NRVB, Nirex Reference Vault Backfill) and a CEBAMA reference cement blend, the last used to facilitate benchmarking among the multinational research teams. Sorption experiments were also performed on carbonated samples of the HCP. The individual mineral phases comprise calcium silicate hydrate (C-S-H), ettringite and monosulphate. These phases were selected as they comprise the major components of a CEM I cement, excluding portlandite as no significant interaction of the latter with radionuclides is expected.

Each HCP above was also employed in the through-diffusion experiments for which solutions pre-equilibrated with the respective cements were prepared. Through-diffusion experiments were performed as described by (Felipe-Sotelo et al., 2014; Hinchliff et al., 2016; van Es et al., 2015). 10 kBq of the radionuclide of interest was spiked into the central well with cement equilibrated water, which was then sealed, and the block placed in equilibrated water (120 cm^3). Movement of radionuclides through the block was monitored by taking 1 cm^3 aquilots of the surrounding water, without replacement, and measuring activity using liquid scintillation counting (LSC). After either the concentration of radionuclides reached steady state, or a specified maximum time (owing to the half-life of ^{125}I), the block was removed from the equilibrated water, sawn axially and the distribution of radionuclides measured by digital autoradiography. The isotopes employed were ^{36}Cl and ^{125}I, as

originally envisaged. Difficulties were encountered in sourcing ^{75}Se. Given that this had been studied previously by the same authors ((Felipe-Sotelo et al., 2014; Hinchliff et al., 2016; van Es et al., 2015) and the acute lack of data for technetium, ^{99}Tc was substituted and the scope extended to include ^{3}H, which was added to emulate a near conservative tracer.

10 Laboratories PSI/EMPA

10.1 Synthesis and characterization of mono-S, mono-Se and mono-I AFm phases

In a first phase of this project pure AFm end members containing one of the following anion species SeO_4^{2-}, SeO_3^{2-}, HSe^-, SO_4^{2-}, SO_3^{2-}, $S_2O_3^{2-}$, HS^-, and I^- were synthesized and characterized by XRD, TGA, DVS, FTIR and Raman spectroscopy. Crystal structure analysis of the synthesized samples revealed the formation of well crystalline AFm phases showing X-ray powder diffraction patterns typical for the AFm family, characterized by strong basal reflections (00l) at low 2Θ values and the (110) diffraction peak at ~31° 2Θ. The S(VI)-AFm and the I-AFm are known to crystallize in the rhombohedral $R\bar{3}$ space group (Allmann, 1977; Rapin et al., 1999) which was also observed in this study. For the S(IV)-AFm the same rhombohedral symmetry consistent with the $R\bar{3}$ space group was determined. These three phases, (I-, S(VI)- and S(IV)-AFm) share a common position of the (110) reflection at about ~31° 2Θ but show differences in the interlayer distances. The corresponding d-spacing are 8.93 Å for the S(VI)-AFm, 8.84 Å for the I-AFm and 8.51 Å for the S(IV)-AFm, respectively. In the Se(IV)-sample the co-existence of two distinct Se(IV)-AFm hydrates with interlayer distances of 11.05 Å and 9.65 Å was found. Different structural organization of the SeO_3^{2-} anion in the interlayer gives rise to two distinct symmetries – a rhombohedral symmetry ($R\bar{3}$) with a larger c axis and Z = 3 for the 11.05 Å hydrate and a trigonal symmetry ($P\bar{3}$) with shorter c axis and Z = 2 for the 9.65 Å hydrate. The Se(VI)-AFm and the S(II)-AFm phases exhibit a lower symmetry, correlating with apparent monoclinic unit cells with the interlayer distances 10.18 Å for the Se(VI)-AFm and 10.33 Å for the S(II)-AFm. Structure refinements for these two phases, however, were only partially successful and the monoclinic structure could not be refined. The observed XRD analysis of the S(-II)-AFm and Se(-II)-AFm, finally, revealed the formation of AFm-like phases with rhombohedral structure. The powder patterns of the samples show the characteristic AFm (110) diffraction peak at about 31° 2Θ as well as the high-intensity basal reflections at low angle. The corresponding interlayer distances are 8.46 Å for the S(-II)-AFm and 8.27 Å for the Se(-II)-AFm.

The hydration states of the samples were determined by TGA analyses. The water removal occurs in several steps which vary in size and range for the different samples. Generally, water loss from the interlayer can be observed in three steps up to a temperature of 250°C; water from the main layer is lost in the temperature region between 250°C and 600°C. A total water content of 10 H_2O for the I-AFm, 11 H_2O for the S(IV)- and Se(IV)-AFm, 12 H_2O for the S(VI)-AFm and 13 H_2O for the S(II)- and Se(VI)-AFm was obtained for samples dried at 8 % relative humidity.

The characterization of the AFm end members was completed with a water sorption study by Dynamic Vapour Sorption (DVS) analysis. The highest hydration level of each sample observed by DVS was then used for the determination of its solubility product (log K) using the thermodynamic modelling software GEMS (Kulik et al., 2013) and the NAGRA/PSI database (Hummel et al., 2002). The following mean values were calculated: -26.9 ± 0.9 (S(IV)-AFm), -27.8 ± 0.5 (I-AFm), -28.4 ± 1.4 (Se(IV)-AFm), 28.5 ± 1.4 (S(VI)-AFm), -29.2 ± 0.6 (Se(VI)-AFm) and -30.5 ± 0.8 (S(II)-AFm).

Sample oxidation during TGA and DVS analyses prevented proper determination of the H_2O content and the solubility product of the S(-II)-AFm and Se(-II)-AFm phases.

10.2 Synthesis and characterization of solid solution series

In a second phase of the project, the formation of binary solid solution of the type SeO_3^{2-}–X^{n-} and I^--X^{n-} (with X^{n-} = SO_4^{2-}, SO_3^{2-}, $S_2O_3^{2-}$, CO_3^{2-}, OH^-) as the intercalating anions was examined. Samples with total selenite (or iodide) mole fraction of $x_{Se(IV)}$ = SeO_3^{2-}/(SeO_3^{2-}+X^{n-}) = 0, 0.1, 0.3, 0.5, 0.7, 0.9 and 1 were synthesized and characterized.

11 References

Atkins, M., Glasser, F.P., 1992. Application of portland cement-based materials to radioactive waste immobilization. Waste Management 12, 105–131. https://doi.org/10.1016/0956-053X(92)90044-J

Atkins, M., Macphee, D., Kindness, A., Glasser, F.P., 1991. Solubility properties of ternary and quaternary compounds in the CaO□Al2O3□SO3□H2O system. Cement and Concrete Research 21, 991–998. https://doi.org/10.1016/0008-8846(91)90058-P

Auroy, M., Poyet, S., Le Bescop, P., Torrenti, J.-M., Charpentier, T., Moskura, M., Bourbon, X., 2018. Comparison between natural and accelerated carbonation (3% CO2): Impact on mineralogy, microstructure, water retention and cracking. Cement and Concrete Research 109, 64–80. https://doi.org/10.1016/j.cemconres.2018.04.012

Auroy, M., Poyet, S., Le Bescop, P., Torrenti, J.-M., Charpentier, T., Moskura, M., Bourbon, X., 2015. Impact of carbonation on unsaturated water transport properties of cement-based materials. Cement and Concrete Research 74, 44–58. https://doi.org/10.1016/j.cemconres.2015.04.002

Baur, I., Keller, P., Mavrocordatos, D., Wehrli, B., Johnson, C.A., 2004. Dissolution-precipitation behaviour of ettringite, monosulfate, and calcium silicate hydrate. Cement and Concrete Research 34, 341–348. https://doi.org/10.1016/j.cemconres.2003.08.016

Bear, I.J., Turnbull, A.G., 1965. The Heats of Formation of Beryllium Compounds . I. Beryllium Hydroxides. J. Phys. Chem. 69, 2828–2833.

Crank, J., 1975. The mathematics of diffusion, 2d ed. ed. Clarendon Press, Oxford, [Eng].

Felipe-Sotelo, M., Hinchliff, J., Drury, D., Evans, N.D.M., Williams, S., Read, D., 2014. Radial diffusion of radiocaesium and radioiodide through cementitious backfill. Physics and Chemistry of the Earth, Parts A/B/C 70–71, 60–70. https://doi.org/10.1016/j.pce.2014.04.001

Giffaut, E., Grivé, M., Blanc, P., Vieillard, P., Colàs, E., Gailhanou, H., Gaboreau, S., Marty, N., Madé, B., Duro, L., 2014. Andra thermodynamic database for performance assessment: ThermoChimie. Applied Geochemistry, Geochemistry for Risk Assessment: Hazardous waste in the Geosphere 49, 225–236. https://doi.org/10.1016/j.apgeochem.2014.05.007

Goñi, S., Guerrero, A., 2003. Accelerated carbonation of Friedel's salt in calcium aluminate cement paste. Cement and Concrete Research 33, 21–26. https://doi.org/10.1016/S0008-8846(02)00910-9

Grivé, M., Duro, L., Colàs, E., Giffaut, E., 2015. Thermodynamic data selection applied to radionuclides and chemotoxic elements: An overview of the ThermoChimie-TDB. Applied Geochemistry 55, 85–94. https://doi.org/10.1016/j.apgeochem.2014.12.017

Hinchliff, J., Evans, N.D.M., Read, D., 2016. Solubility constraints affecting the migration of selenium through the cementitious backfill of a geological disposal facility 305, 21–29.

JCPDS, 2001. Powder diffraction files, Joint Committee on Powder Diffraction Standards. Swarthmore, USA.

Lange, S., 2019. Structural uptake and retention of safety relevant radionuclides by cementitious materials, PhD Thesis, RWTH Aachen University [WWW Document]. URL https://juser.fz-juelich.de/record/866226/files/Energie_Umwelt_480.pdf (accessed 11.21.19).

Lange, S., Kowalski, P.M., Pšenička, M., Klinkenberg, M., Rohmen, S., Bosbach, D., Deissmann, G., 2018. Uptake of 226Ra in cementitious systems: A complementary solution chemistry and atomistic simulation study. Applied Geochemistry 96, 204–216. https://doi.org/10.1016/j.apgeochem.2018.06.015

Marty, N.C.M., Grangeon, S., Warmont, F., Lerouge, C., 2015. Alteration of nanocrystalline calcium silicate hydrate (C-S-H) at pH 9.2 and room temperature: a combined mineralogical and chemical study. Mineralogical Magazine 79, 437–458. https://doi.org/10.1180/minmag.2015.079.2.20

Matschei, T., Lothenbach, B., Glasser, F.P., 2007. The AFm phase in Portland cement. Cement and Concrete Research 37, 118–130. https://doi.org/10.1016/j.cemconres.2006.10.010

Metz, V., Ganor, J., 2001. Stirring effect on kaolinite dissolution rate. Geochimica et Cosmochimica Acta 65, 3475. https://doi.org/10.1016/S0016-7037(01)00686-X

Ochs, M., Mailants, D., Wang,L., 2016. Radionuclide and Metal Sorption on Cement and Concrete. Springer, Cham.

Parkhurst, D.L., Appelo, C.A.J., 2013. Description of input and examples for PHREEQC version 3—a computer program for speciation, batch-reaction, one-dimensional transport, and inverse geochemical calculations. US Geological Survey Techniques and Methods, book 6, chap A43, p 497. Available only at <http://pubs.usgs.gov/tm/06/a43 | Request PDF [WWW Document]. ResearchGate. URL https://www.researchgate.net/publication/273125712_Parkhurst_DL_Appelo_CAJ_2013_Description_of_input_and_examples_for_PHREEQC_version_3-a_computer_program_for_speciation_batch-reaction_one-dimensional_transport_and_inverse_geochemical_calculations_US_ (accessed 11.21.19).

Perkins, R.B., Palmer, C.D., 1999. Solubility of ettringite (Ca6[Al(OH)6]2(SO4)3 · 26H2O) at 5–75°C. Geochimica et Cosmochimica Acta 63, 1969–1980. https://doi.org/10.1016/S0016-7037(99)00078-2

Pointeau, I., Landesman, C., Giffaut, E., Reiller, P., 2004. Reproducibility of the uptake of U(VI) onto degraded cement pastes and calcium silicate hydrate phases. Radiochimica Acta 92. https://doi.org/10.1524/ract.92.9.645.55008

Savoye, S., Page, J., Puente, C., Imbert, C., Coelho, D., 2010. New Experimental Approach for Studying Diffusion through an Intact and Unsaturated Medium: A Case Study with Callovo-Oxfordian Argillite. Environ. Sci. Technol. 44, 3698–3704. https://doi.org/10.1021/es903738t

Savoye, S., Rajyaguru, A., Macé, N., Lefèvre, S., Spir, G., Robinet, J.C., 2018. How mobile is tritiated water through unsaturated cement-based materials? New insights from two complementary approaches. Appl Radiat Isot 139, 98–106. https://doi.org/10.1016/j.apradiso.2018.04.019

van Es, E., Hinchliff, J., Felipe-Sotelo, M., Milodowski, A.E., Field, L.P., Evans, N.D.M., Read, D., 2015. Retention of chlorine-36 by a cementitious backfill. Mineralogical Magazine 79, 1297–1305. https://doi.org/10.1180/minmag.2015.079.6.05